Study of Shock Formation Parameters With Drive Conditions in Magnetically Accelerated Plasma Flows

Simon C. Bott-Suzuki, *Senior Member, IEEE*, Maria Pia Valdivia, *Member, IEEE*, Jacob T. Banasek, *Member, IEEE*, Samuel W. Cordaro, *Member, IEEE*, Ann Truong, Hanyu Hu, Chin-Chou Wu, Noah Dilworth, B. R. Kusse, D. A. Hammer, *Life Fellow, IEEE*, Eric Sander Lavine, *Member, IEEE*, W. M. Potter, *Member, IEEE*, J. B. Greenly, and Felipe Veloso, *Member, IEEE*

***Abstract*— We present experimental data regarding the formation of high-energy-density shocks in magnetically accelerated plasma flows using pulsed power drivers. We quantify the flow velocity and temperature of the ablated plasma using optical Thomson scattering and gated emission imaging across two different generators. We show that, regardless of the drive parameters, the plasma flows show continuous acceleration over centimeter spatial scales, in line with trends in published simulation work. When stationary targets are placed in these supersonic flows, bow-shock formation is observed at all drive parameters in a range of materials. In the higher density flow generated on the 1-MA COBRA generator at Cornell University, heating of the upstream flow ahead of the shock is observed and quantified, which is not observed at the lower density flow on the 0.2-MA Bertha driver at UC San Diego. When combined with previous work on the XP generator at Cornell, we can show that these three experimental setups allow control of the effect of radiation loss and upstream absorption on the formation of the bow shock.**

***Index Terms*— High-energy-density physics, pulsed power, shock formation.**

I. Introduction

SHOCK formation is common in a number of hydrodynamic and plasma systems. As large-scale drivers become increasingly available for high-energy-density studies, accurate quantification of the process that controls shock formation and evolution is needed. There are a number of unanswered questions about strong shock formation, including multiple shock interactions [1], [2], Mach stem formation [3], [4], and the equation of state for highly compressed media [5], [6]. Such plasmas are present in several inertial confinement fusion systems [7], [8], [9] as well as in a wide range so astrophysical contexts [10], [11], [12], [13], [14], and advancing the numerical work used to analyze and scale plasmas in this regime requires high-quality experimental data wherever possible.

A key component of the development of accurate predictable simulations is obtaining sufficiently broad, detailed, and quantified experimental data against which numerical work can be benchmarked. Within several areas of high-energy-density physics and related areas, there is a need to recover novel information and provide data with error bars to support simulation efforts. This is especially important where radiation and transient magnetic fields influence energy redistribution and system evolution.

In this work, we present data from ablating inverse wire arrays [15]. We quantify the velocity and temperature profile for a range of experiments initially without obstructions, to examine the flow conditions, and then with obstructions to study shock formation. We examine the shock structure and the flow upstream of the shock to examine the role of radiation transport. This becomes increasingly important as the upstream density increases, achieved experimentally by increasing the driver peak current in scaled experiments across different facilities.

II. Experimental Setup

Experiments using inverse or exploding wire arrays were carried out on two pulsed power drivers using similar setups and diagnostics to allow comparison of shock formation. The drivers were Bertha at UC San Diego (200 kA and 1100 ns [16]) and COBRA (1 MA and 100 ns [17]) at Cornell University. The load setup comprises a central cathode stalk, from which two thin metallic wires are hung, connecting with two return electrodes at the electrical ground. The wires are made from typically mid-Z to high-Z metals, primarily tungsten for these studies. As the drive current is applied, the magnetic field around the central cathode interacts with the

Manuscript received 30 November 2023; revised 8 April 2024 and 13 May 2024; accepted 5 August 2024. This work was supported in part by the National Nuclear Security Administration (NNSA) Stewardship Science Academic Alliances (SSAA) under DOE Cooperative Agreement DE-FC03-02NA00057 and in part by the Sandia under Contract 2342454. The work of F. Veloso was supported by the Fondecyt/Regular under Project 1231286. The review of this article was arranged by Senior Editor F. Beg. *(Corresponding author: Simon C.Bott-Suzuki.)*

Simon C. Bott-Suzuki, Maria Pia Valdivia, Ann Truong, Hanyu Hu, Chin-Chou Wu, and Noah Dilworth are with the Center for Energy Research, University of California San Diego, La Jolla, CA 92093 USA (e-mail: sbottsuzuki@ucsd.edu).

Jacob T. Banasek and Samuel W. Cordaro are with Sandia National Laboratories, Albuquerque, NM 87185 USA.

B. R. Kusse is with the School of Applied and Engineering Physics (AEP), Cornell University, Ithaca, NY 14850 USA.

D. A. Hammer, Eric Sander Lavine, W. M. Potter, and J. B. Greenly are with the School of Electrical and Computer Engineering, Cornell University, Ithaca, NY 14850 USA.

Felipe Veloso is with the Physics Department, Pontificia Universidad Católica de Chile, Santiago 7820436, Chile.

Color versions of one or more figures in this article are available at https://doi.org/10.1109/TPS.2024.3442748.

Digital Object Identifier 10.1109/TPS.2024.3442748

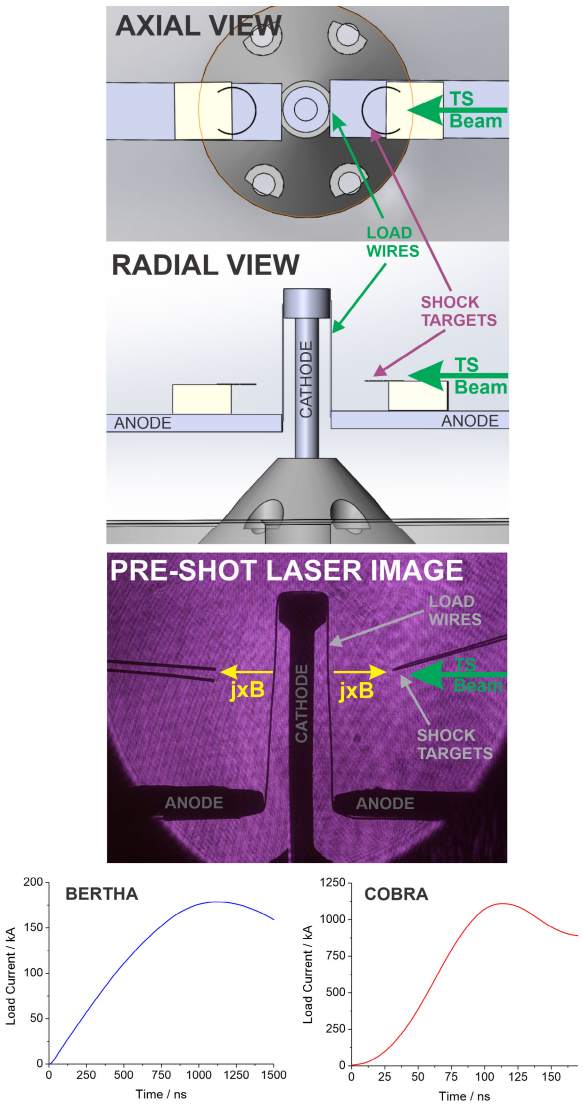

Fig. 1. Schematics of inverse (or exploding) wire array showing both axial and radial views, along with laser shadow image of an example load on Bertha, and typical load currents for Bertha and COBRA shots.

current density in each wire to generate a radially outward Lorentz force. The plasma ablated from each wire is accelerated by this force to supersonic, and often super-alfvenic, velocities. The general setup is shown in Fig. 1. Given the lower current on Bertha compared to COBRA, the experiment is scaled; the top cathode diameter for COBRA and Bertha is 8 and 4 mm, respectively, with all other dimensions scaled similarly. The important parameter here is the ratio of the global B-field generated by the central electrode post to the local field generated around the wire. If this is strongly in favor of the local field (i.e., $B_{\text{local}} \gg B_{\text{global}}$), plasma is constricted to the wire and the expected $m = 0$ magnetohydrodynamic instabilities are observed, with little plasma accelerated away. If the local field is sufficiently reduced, for example, by using more than one load wire in parallel, the typical ablation process is observed [18], and plasma is accelerated radially outward from the load wires. The ablation process occurs similarly for wire array loads from tens of kiloamperes to many MA, and scaling parameters are observed to be generally invariant with the current level [18], [19], [20], [21].

For inverse wire arrays in this work, accelerated flow densities typically have $n_e = 10^{17}$–10^{18} cm^{-3} and $T_e \sim 15$ eV [7], [8]. In shock regions, densities rise by a factor of 4 or more, and temperatures reach 50 eV or greater depending on the experiment. Flow velocities are typically >20 km/s with sonic Mach numbers >2, and thus, the flows expand only slowly perpendicular to their velocity. A quasi-2-D plasma sheet results, in which shocks are readily formed by placing stationary targets in the path of the flow. These targets are wire loops ~ 50 μm in diameter that pass through the plasma flow at one radial position. The loops are mounted on an electrically insulated mount (Delrin), to eliminate the possibility of current flow in the targets themselves.

Previous studies of a similar experiment on the XP generator [22] investigated shock formation and quantified the Mach number and plasma compressibility γ and determined that the shock formation in these experiments is primarily hydrodynamic. While B-field convected with the flow in these resistive plasmas is not negligible, the high plasma β in the shock means that it does not play a significant role in dynamics. This is demonstrated to be the case for these new experiments in Section III.

For the present studies, we primarily use Thomson scattering diagnostics combined with laser imaging (shadowgraphy and interferometry) and gated soft X-ray imaging using microchannel plates. Data from Thomson scattering measurements are analyzed using the ThomsonPy code [23], which has been used to examine plasma jets [24], [25], inverse wire arrays [16], and sheared flow Z-pinches [26]. The code simulates noncollisional spectra using the experimental scattering geometry, which is iteratively fit to the data. Errors are determined using a Monte Carlo method of 1000 fits allowing the details of the collection and spectrometer to vary in a narrow range around the measured values. Interferometry data are analyzed using the Talbot numerical tool (TNT) [27]. This is a postprocessing module of the Talbot Interferometry Analysis (TIA) code [28] and was used to separate the different Fourier components of both the data and reference images. This tool has been developed to automatically detect the peaks corresponding to the periodicity of the fringes in the Fourier spectra, particularly for noisy images, or low-fringe-contrast data. The unwrap routine is robust to the presence of fringe errors and experimental details (e.g., electrodes and targets), maintaining high spatial and frequency resolution. Errors in measured values are a function of the fit to the analyzed fringe pattern for the routine employed. TNT uses a 12-point fit per 2π period, and therefore, areal electron densities are determined to be within 1/12 of a fringe shift, for a measurement error of $(n_{e,\text{areal}}) \pm 0.08 \times 10^{17}$ electrons/cm^2 for the system used here (see also Valdivia et al. [29], this volume).

In this work, we quantitatively characterize details of the undisturbed ablated plasma flow from the load wires on both Bertha and COBRA, examine shock formation in these flows, and then compare results to both previous work on XP and analytical calculations of the expected shock properties.

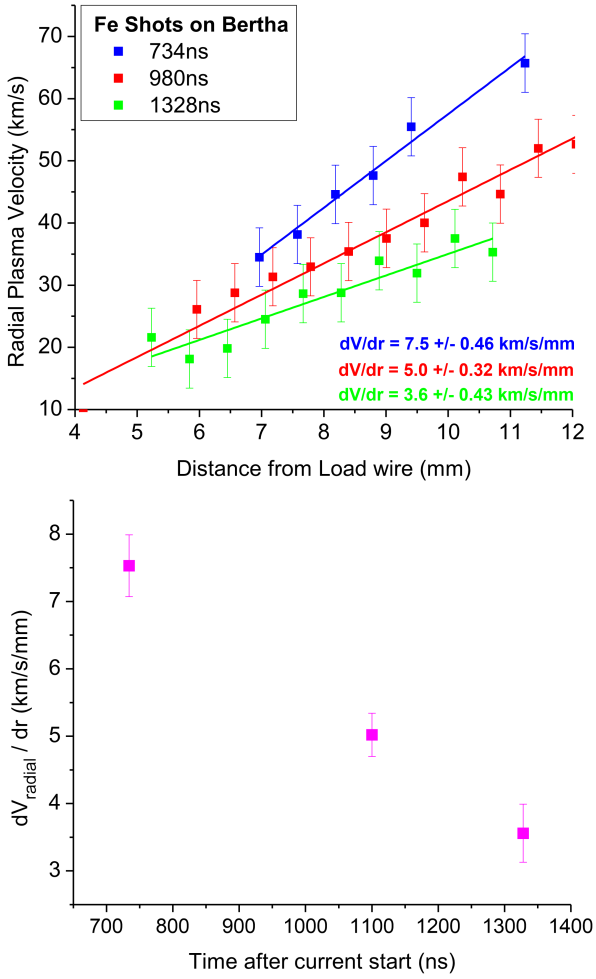

Fig. 2. Evolution of the plasma radial velocity profile for Fe shots on Bertha (top) and change of the fit velocity gradient with time (bottom).

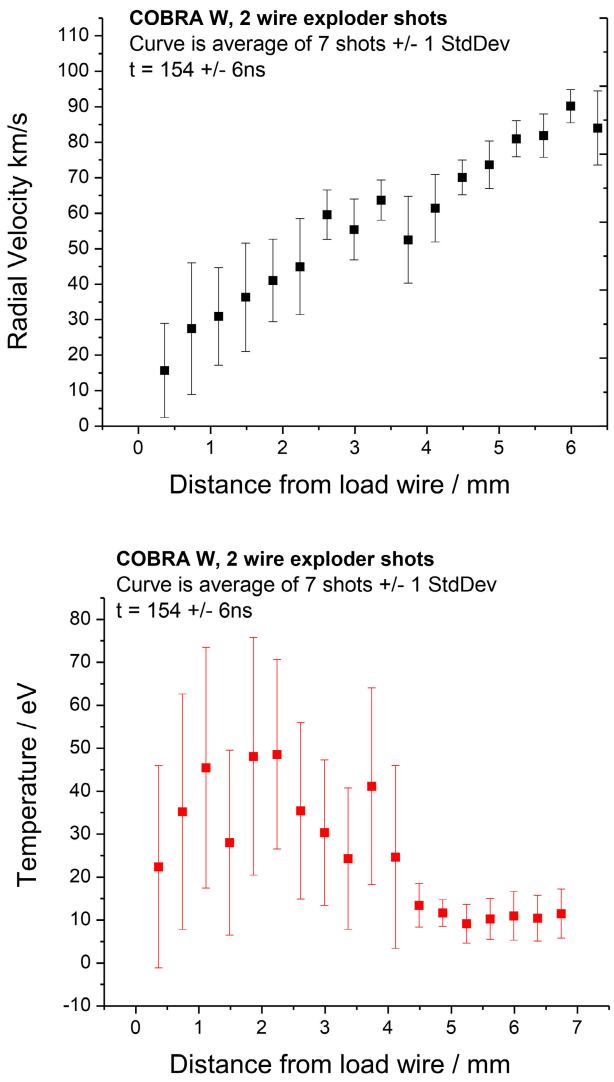

Fig. 3. Plots of the radial velocity and temperature profile determined from Thomson scattering data for seven shots using W array at 154 ns on COBRA.

III. Characterization of Accelerated Plasma Flows

The moderately sized pulsed power drivers employed here carry out experiments three or more times per day. The advantage of this is that baseline experiments can readily be carried out. We first examine the accelerated plasma flow on Bertha and COBRA as initial conditions for the shock work presented in Section IV. Thomson scattering is carried out where the laser is incident anti-parallel to the plasma velocity, indicated in Fig. 1, with collection at 90° (COBRA) or 135° (Bertha) relative to the laser propagation direction. Flow velocities are then determined from the Doppler shift relative to the laser signal and electron temperatures by peak separation using the ThomsonPy code. Note that temperature determination for Bertha experiments is not possible due to the poor signal-to-noise ratio.

Experiments on Bertha examined the radial velocity profile along with its temporal evolution for W experiments. Thomson scattering data were taken close to peak current time to maximize the scattering signal. Velocity data from fits of the Doppler shift are plotted in Fig. 2.

The plasma continuously accelerates as it travels radially outward from the load wire, likely as a result of convection of the drive current. Velocity profiles at all times appear linear with position. At the earliest times measured, the velocity peaks at 65 km/s at 11 mm from the wires. This profile is qualitatively similar to that predicted by magnetohydrodynamic simulations of converging wire arrays driven by similar ablation processes [30]. Later in time, the velocity profile is reduced for all radial positions, with measurement after peak current only reaching 35 km/s. Given that the wire material does not appear to change the measured velocity, as shown in [16], all experiments with a similar experimental setup would be expected to follow this trend. The lower plot in Fig. 2 shows the fit velocity gradient for each of the three times examined, which monotonically decreases with time.

For COBRA experiments at 1 MA, both the radial velocity and temperature can be quantified using the Thomson scattering system. A series of seven identical experiments were carried out with W arrays. Fig. 3 shows an average over all seven shots for velocity and temperature at 18 radial locations taken at the same time in the current pulse. The error bars on the plot represent the variation in the fit parameters over the seven shots examined, which dominates over the error in the fit from the Thomson data.

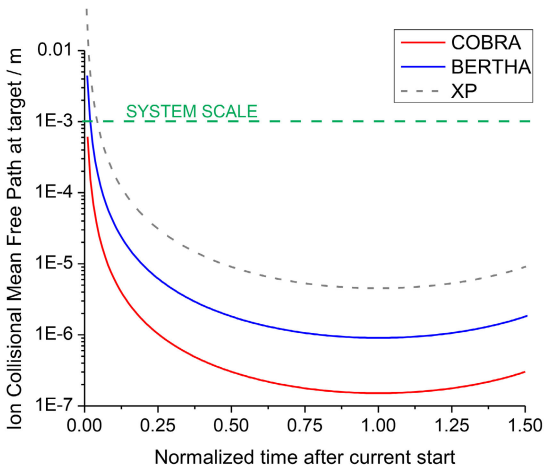

Fig. 4. Comparison of the collisional ion mean free path at a target 5 mm from the load wire for COBRA, Bertha, and XP experiments, plotted as a function of time normalized to peak current.

The radial velocity profile shows a similar continuous acceleration throughout the measured locations as the plasma moves away from the load wire, reaching 90 km/s at 6 mm. The variability, denoted by the error bars, reduces significantly at larger radial positions and is typically <10% far from the wire.

The radial temperature profile shows two clearly delineated regions. Less than 4 mm from the load wire, plasma temperatures reach 50 eV and show strong variability shot-to-shot, with error bars over 75% of the inferred temperature in several locations. At locations greater than 4 mm from the load wire, the temperature is significantly reduced, remaining relative constant at 10–15 eV, and shows far less variability, at least in absolute terms. The clear distinction observed with radial position likely directly reports the limit to radial convection of the drive current in the plasma.

At similar radial positions and similar times relative to peak current, the absolute value of the flow velocity is higher by about a factor of 4 on COBRA relative to Bertha; Bertha values are ∼20 km/s at 6 mm from wire at 1300 ns (120% of peak time) versus 85 km/s on COBRA at 6 mm from load wire at 154 ns (146% of peak time). Given that the "ablation velocity" is typically invariant over a number of experiments [15], [18], [19], [20], [21], [22], we attribute this primarily to the significantly longer rise time in the Bertha experiments (x10) compared to the COBRA experiments. This work is the first to provide quantitative data on such long-rise time experiments, and further work is needed to confirm this thesis.

From analytical calculations along with the data recovered, we can also plot various parameters of the generated plasma flow to determine the dominant physics. In Figs. 4 and 5, we plot the collisional ion mean free path, as well as the Reynolds number (Re) and the magnetic Reynolds number (Re_M). The collisional ion mean free path determines if a fluid treatment of the flow is appropriate relative to the various system scales. This is shown in Fig. 4 for the Bertha and COBRA experiments as well as the XP data presented in [22], using the methods in [15]. The ion mean free path is calculated

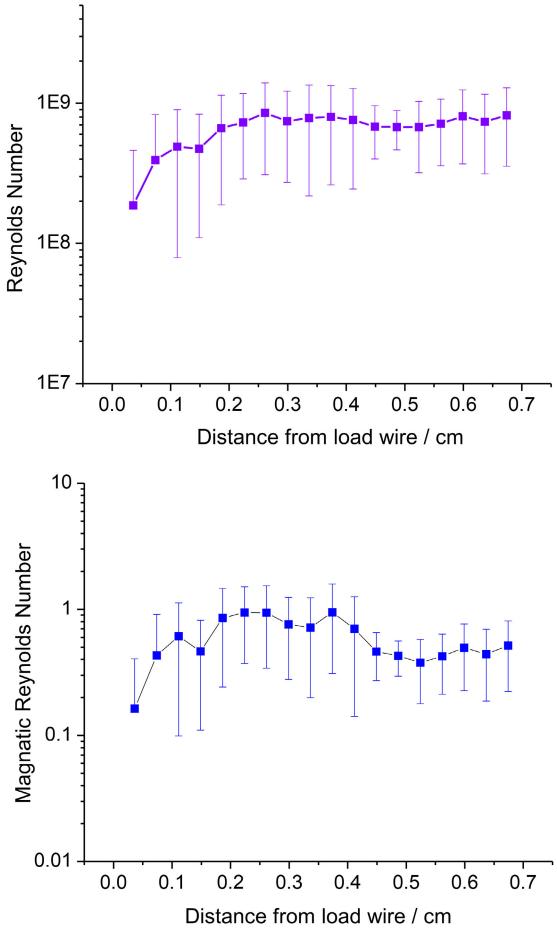

Fig. 5. Plots of (top) the flow Reynolds number and (bottom) the flow magnetic Reynolds number for tungsten experiments on COBRA at 154 ns using velocity and temperature data from Fig. 3.

as a function of time at a target location 5 mm from a tungsten load wire. Note that the time scale is normalized to the peak current on each driver to allow a direct comparison.

For all three drivers, the ion mean free path rapidly drops below a "system scale" of 1 mm, and by the time of shock formation and measurement (close to peak current), this is below 10 μm for XP and even less for Betha and COBRA. This is smaller than any feature in the experiment, and therefore, fluid dynamics calculations are appropriate.

The calculations for Re and Re_M require temperature data to calculate the kinematic viscosity and magnetic diffusivity respectively. This is only available for COBRA experiments, and therefore, we only carry out calculations for COBRA, although we expect XP and Bertha plasmas to show similar values. Fig. 5 shows the calculated Re and Re_M values at 154 ns for the COBRA tungsten experiment, using the data from Fig. 3. As can be seen, the Reynolds number is very high ($>10^8$) at all spatial locations at this time and viscosity plays little role in the flow. The magnetic Reynolds number increases in the initial 1 mm from the load wire, reaching ∼1 at 2–4 mm, before reducing to ∼0.5 at distances greater than 4 mm.

Given that the magnetic Reynolds number is of order 1, there remains the possibility of magnetic field being convected in the flow and playing a role in the shock formation or

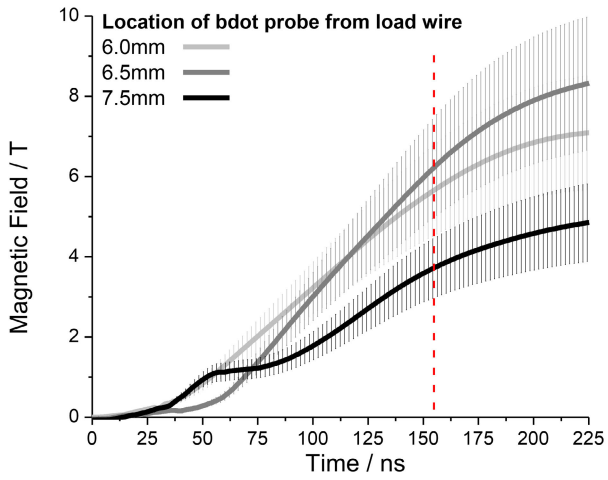

Fig. 6. Traces from magnetic field probes placed in the plasma flow at different locations for COBRA shots with no shock targets. Solid lines are the data for three locations as a function of time, and the shaded areas are the uncertainties in the measurements. Vertical dotted line is the experimental time for the data in Fig. 3.

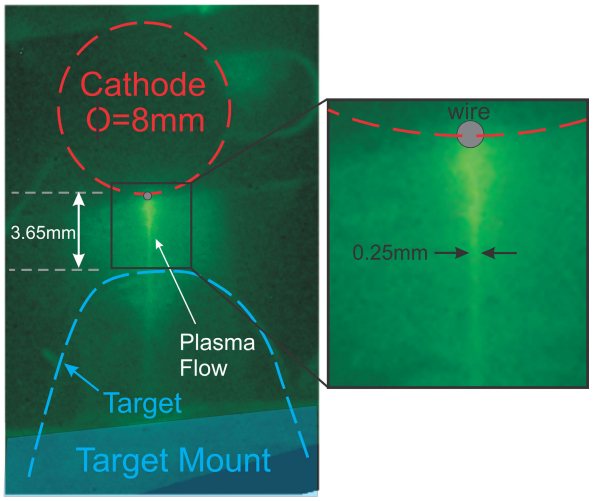

Fig. 7. Axial gated emission imaging from COBRA experiments at 80 ns showing plasma accelerated from load wires, with a radial dimension of ~250 μm.

structure. The shock formation is driven by the plasma flow pressure, also termed the kinetic ram pressure, so in order to be dynamically significant, the magnetic field pressure at the target location must be comparable to this ram pressure; β in this case is $\beta_{\text{kinetic}} = \rho V^2/(B^2/2\mu_0)$. Using magnetic field probes (B-dots) placed in the plasma flow for shot with no targets on COBRA, the B-field variation with time can be measured at several radial positions, which is shown in Fig. 6.

At 6 mm, close to the location of the targets in all shots presented, the B-field reaches ~6 T at the time of the experimental data on COBRA shots (~150 ns). At this time, the plasma upstream flow density is ~6 mg/cc (n_e ~2×10^{19} cm^{-3}) and velocity ~70 km/s. Calculating β_{kinetic}, we find that this is ~7000 (i.e., strongly dominated by hydrodynamics). The B-field would have to be 250 T to be important at the 10% level.

From Fig. 6, we have the measure of the peak shock temperature of ~45 eV, and we can estimate a regular thermal plasma β too. In this case, $\beta_{\text{thermal}} = (Z+1)\text{nKT}/(B^2/2\mu_0) \sim 100$, where $Z = 25$ for W at 45 eV. A magnetic field of ~30 T is required to be important at the 10% level. These values are in agreement with a similar discussion from [22] from our earlier work on the XP generator.

Given that the experiments are scaled as discussed above, it would be expected that these relationships generally hold for the Bertha experiments presented. In both the kinetic and thermal β cases, the plasma pressures dominate the magnetic pressure, and the B-field is not significant in the shock formation at the location where the targets are fielded in this work.

IV. Comparison of Shock Formation Across Pulsed Power Driver Parameters

Following characterization of the flow, shock experiments were carried out. The shock targets described in Fig. 1 were typically placed at least 4 mm from the load wire, to avoid the strongly heated region observed in the COBRA experiments. This limits possible current flow close to the target and reduces the effect of entrained B-field, so it is dynamically insignificant as discussed above. The very limited azimuthal expansion of the accelerated plasma "sheet" can be observed using gated self-emission imaging taken axially (i.e., from the axial view in Fig. 1). This uses an MCP detector on a pinhole camera arrangement, which is gated at 5 ns and sensitive to radiation >20 eV. An example is shown in Fig. 7. The circular cathode post is visible, as is the loop wire target. The bright plasma stream extends from the cathode and past the target, impacting it in one position. The cathode diameter in the image is 8 mm, and the azimuthal expansion of the plasma flow is ~0.25 mm.

For COBRA experiments, qualitative information can be obtained using the same gated self-emission diagnostic from the radial direction. Experiments using a range of materials were carried out to examine the general form of the shock in each case. Fig. 8 shows shock formation around peak current on COBRA for Ti, Mo, and W load wires impacting the same 50-μm W targets. For reference, an experiment using a Ti load with no target is also shown. The load wire appears on the right of the images with the flow acceleration from right to left, impacting the target outlined by the orange line. In each case, a clear Mach cone is distinguishable, denoting a Mach number ~3–4. The shock is strongly emitting both at the apex and along the wings, as well as slightly ahead of the target position itself.

For more quantitative measurements, the Thomson scattering system can again be applied. For W experiments close to peak current, both the temperature and velocity are recoverable, and an example is shown in Fig. 9. The velocity profile shows an increase from only a few km/s close to the wire to about 60 km/s at the target. As the flow crosses the shock region, the velocity drops slightly before rising again as the flow expands in the Mach cone region. The temperature profile shows a number of interesting features. The plasma is heated to 20 eV close to the wire, cooling rapidly to 10 eV after 2 mm. The temperature then begins to slowly rise before peaking at ~40 eV over the shock and cooling strongly to 5 eV behind it. Notably, the increase in temperature ahead of the

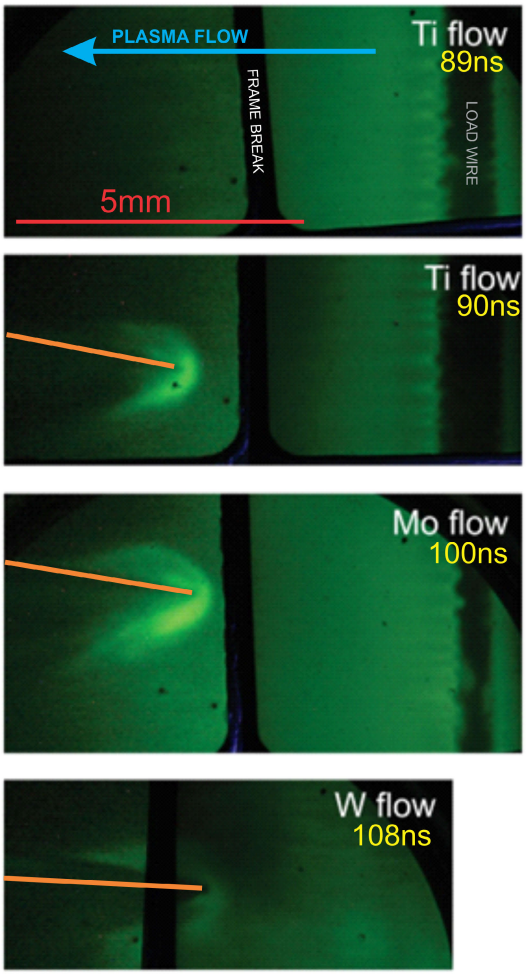

Fig. 8. Gated self-emission images of different loads showing shock formation of COBRA. Top: Ti flow with no target, followed by Ti, Mo, and W experiments with shock targets. All images are scaled identically, and the spatial scale for the upper Ti image applies to all.

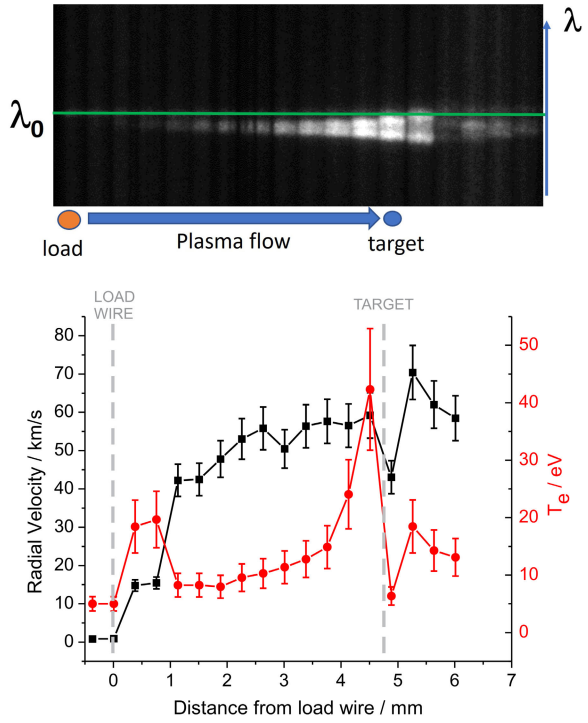

Fig. 9. Thomson scattering data from W array on COBRA at 167-ns (top) raw data and (bottom) fit velocity and temperature against the radial position, showing upstream heating of plasma flow ahead of strong shock location.

shock begins ∼2 mm ahead of the target/shock position. As discussed in [22], all the flows here are strongly collisional and the ion mean free path is significantly less than feature spatial scales ($\lambda_{\text{ion}} \ll 100\ \mu$m, Fig. 4). The electron mean free path is smaller than this by approximately the ratio of masses $m_{\text{ion}}/m_{\text{electron}}$, and therefore, any upstream heating is not caused by heat convection by the electron population.

It should be noted that previous work showed that the Cornell–Thomson scattering probe laser beam can cause localized heating of the plasma, complicating temperature measurements [24]. In that work, inverse Bremsstrahlung was shown to heat the electron population during the measurement period.

In this work, a clear nonuniform temperature profile was observed in both the shock and nonshock experiments (Figs. 3 and 9). The Thomson probe laser is incident from a large radius toward the experiment axis (i.e., from right to left in Figs. 3, 8, and 9, as shown in Fig. 1). When the shock is formed, the laser, therefore, travels from the high-density region behind the shock, through the shock front and into the low-density upstream region. Since heating by the Thomson probe beam would be by inverse bremsstrahlung process, which is proportional to $n_e n_i$, higher density regions should heat more strongly. However, we see that the high-density region behind the shock cools very strongly on the Thomson scattering data (Fig. 9), in agreement with the imaging data (Fig. 8). This demonstrates that the plasma temperature is not being perturbed by the probe beam.

If laser heating of the plasma were occurring, we might also expect significantly elevated temperatures over those typically observed for wire array experiments. However, the shock temperatures measured by Thomson scattering here are in line with temperatures of 40–50 eV inferred from the earlier XP experiments [22] and counter-propagating flow collisions [31], [32], which did not use a Thomson scattering diagnostic. Therefore, it is reasonable to assume that the effect of probe beam heating in these COBRA experiments is very limited.

By contrast to the COBRA shots, similar shock experiments on Bertha at lower upstream density do not show such heating features either qualitatively or quantitatively. Gated self-emission images do not show similar upstream intensity ahead of the shock wings. While Thomson scattering measurements of T_e are not available, interferometry does not show an increase in ionization upstream of the flow even at peak current on Bertha. In fact, the shock jump remains very pronounced throughout the observed shock timescale. Fig. 10 shows an example of interferometry data from W experiments on Bertha. Again, the shock Mach cone is clearly discernable, indicating $M \sim 2.8$ in this case. The interferometry unfold allows a quantitative lineout along the flow direction to be taken. The electron density drops away from the load wire and remains constant at $\sim 7.5 \times 10^{16}$ cm^{-2} until very close to the indicated target position. There is no increase in ionization as the target is approached and clearly not on the spatial scales observed for COBRA shots.

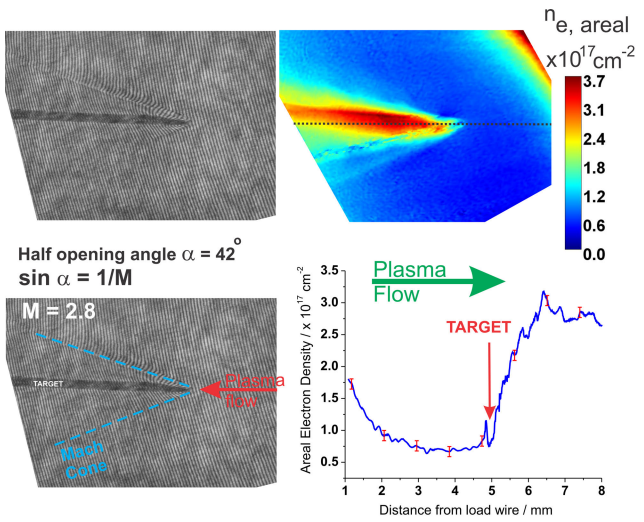

Fig. 10. Magnified view of shock formation for W array on Bertha at 710 ns. Raw data, Mach cone determined from interferometry data, TNT unfold, and lineout through shock are shown. Error bars are indicated as 1/12 fringe shift as discussed in the text.

The data from COBRA and Bertha experiments clearly show differences in behavior ahead of the shock region defined by the target location. Qualitative data from self-emission imaging is supported by quantitative measurements. This suggests that the upstream flow parameters have a significant effect on the shock structure evolution. It is feasible that the radiation from the shock is absorbed by the upstream plasma flow. The data presented demonstrate that upstream heating features are only seen in the most dense experiments on COBRA, and therefore, there is a clear dependence on the upstream characteristics. We investigate the likelihood of radiation-driven heating in the next section.

V. Calculations and Discussion

As was applied in [22], we can use the analytical formulas from [33] and [34], [35] to determine whether the shocks generated in these experiments are expected to be in a regime where radiative effects are important. Values calculated for shock strength parameter Q and the "radiative" parameter R_r can be calculated from the equations below (note that temperatures are taken in eV rather than degrees K)

$$Q = \frac{2\sigma u_s^5}{R^4 \rho_0} \tag{1}$$

where σ is Stefan–Boltzmann's constant (5.67×10^{11} erg/cm^2/s/eV^{-4}), R is the gas constant (8.31×10^{10} erg/g/eV), u_s is the shock speed in cm/s (for the stationary shocks here, this is the measured upstream velocity), and ρ_0 is the upstream mass density in g/cm^3. For radiative effect to be important, this requires $Q > 5 \times 10^3$ for $\gamma = 4/3$ or > 800 for $\gamma = 5/3$.

The "radiative" parameter is defined as

$$R_r = \frac{64}{\gamma(\gamma+1)} \frac{\sigma}{c_v^4} \frac{u_s}{\rho_0} \tag{2}$$

where Stefan–Boltzmann's constant $\sigma = 5.67 \times 10^{-8}$, c_v is the specific heat, u_s is the shock velocity in m/s, and ρ_0 is the flow density in mg/cc. For radiative effect to be important, this requires $R_r > 1$. For these parameters, the most strongly varying values, and those most relevant to shock formation, are the upstream flow velocity and density. Over the three experiments, density changes from ~0.05 mg/cm^3 for Bertha at 200 kA to ~6 mg/cm^3 for COBRA experiments. Velocities are in the range 10–90 km/s. We also include values from the previous XP experiments in [22]. We can plot the parameter space for Q and R_r as a function of these and this is shown in Fig. 11.

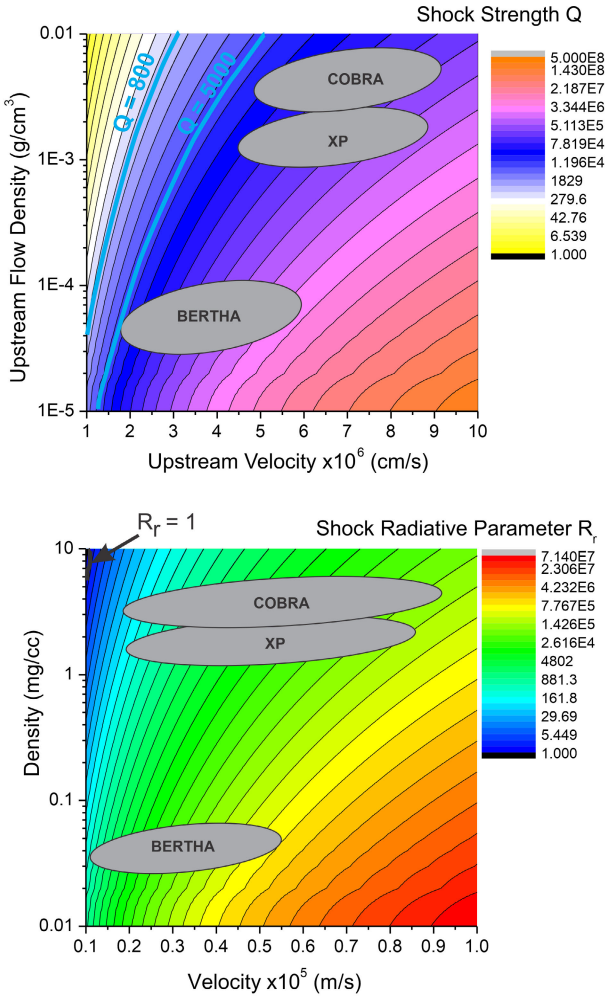

Fig. 11. Contour plots on (top) of the shock strength parameter Q and (bottom) shock radiative parameter R_r with flow density and velocity. Areas indicated by gray shapes are the ranges of Q covered by the three experimental datasets.

On the R_r plot (lower in Fig. 11), the left-hand side of the ranges for each experiment is for $\gamma = 5/3$ and the right-hand side is for $\gamma = 4/3$, which is more appropriate for the denser experiments on XP and COBRA. Note that both plots vary as u_s^5/ρ_0, so the contours' shapes are similar with a different scaling factor. It is clear that for all three experimental datasets, the required values for Q and R_r are met. In fact, over a wide range of values using the inverse wire array shock platform, both these are readily exceeded. The values calculated are plotted in Fig. 12.

It remains to determine the differences between the experiments presented as well as previous data presented in [22]. A factor in the analysis is the photon mean free path

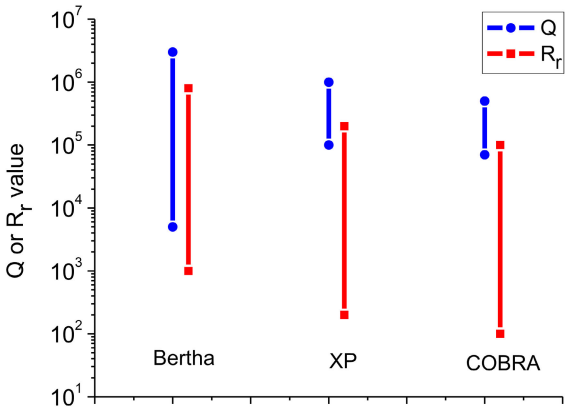

Fig. 12. Plot of the range of the Q and R_r parameters over experiments on the three pulsed power drivers discussed.

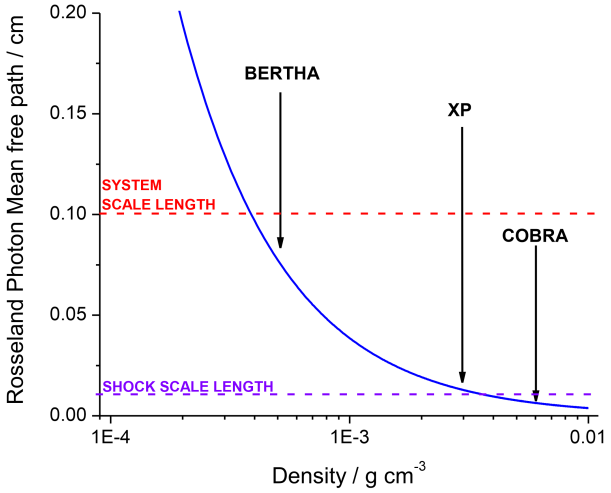

Fig. 13. Plot of the photon mean free path against flow density with important scale lengths and experimental parameter ranges for all three drivers indicated.

(or equivalently, the opacity) of the upstream flow to the radiation emitted from the shock region. If this is small compared to the shock scale lengths (~100 μm), we might expect radiation to be important immediately upstream of the shock. If this is more comparable to the system scale length (~1 mm), we might expect this effect to be limited. Data in [22, Fig. 11] is interesting in the sense that radiative precursor formation was questionable but showed suggestions of limited heating upstream of the shock in imaging data.

We can calculate the photon mean free path using the Rosseland mean opacity. There are simplified formulas available for such calculations that provide good fits to the full calculated opacities for different densities, temperatures, and materials (e.g., [36]). The mean opacity K is

$$K = aT^s\rho^r \tag{3}$$

where T is the temperature in keV; ρ is the density is g/cm^3; and a, s, and r are constants from the fitting process. For W, $a = 244.12$, $s = -1.119$, and $r = 0.005$, and for Al, $a = 3.78$, $s = -2.482$, and $r = 0.481$. From this, the photon mean free path l_{photon} is

$$l_{\text{photon}} = \frac{1}{K\rho}. \tag{4}$$

A plot of the photon mean free path as a function of density using $T = 0.015$ keV for all cases is shown in Fig. 13. Arrows indicate the approximate ranges for each of the three experiments, with density values taken directly from experimental values.

For the most dense experiments on COBRA, the photon mean free path is short compared to the shock scale length, and therefore, it is reasonable to expect radiation absorption in the upstream flow. This absorption will drive an increase in the plasma temperature ahead of the shock for some limited range depending on the flux. This is in agreement with the Thomson scattering data presented in Fig. 9. For the least dense experiments on Bertha, the photon mean free path is close to the system scale length of ~1 mm, so radiation will likely not play a significant role in the upstream flow evolution. The XP experiments are intermediate between these extremes, with l_{photon} of the same scale as the shock features. This perhaps explains why those experiments were inconclusive, motivating the work presented here.

We recognize that these simplified calculations do not capture the complex physics of this system, but they do give a guide as to why the experimental observables are different. Future experiments will further examine the evolution of this shock system in dense flows to provide more detailed analyses for comparison to calculations. As noted above, the data here from both shock and no shock experiments will serve as benchmarks for on-going simulation work, which will be presented in future publications.

VI. Conclusion

We have presented new experimental data from inverse wire array experiments on two pulsed power drivers: Bertha (200 kA, 1100 ns) at UC San Diego: and COBRA (1 MA, 100 ns) at Cornell. For experiments examining the undisturbed plasma outflow, both sets of experiments show continuous acceleration of the plasma up to 1 cm from the load wire, in line with both previously published and current simulation work. It is also observed for Betha experiments that the flow velocity varied with time, but not material, with the measured radial acceleration reducing with increasing time. The absolute values of the flow velocities are different on the two generators, with COBRA experiments being higher than Bertha experiments by about a factor of 4. We attribute this primarily to the significantly longer rise time in the Bertha experiments (x10) compared to the COBRA experiments. Strong heating, likely due to current convection with the flow, is observed up to 4 mm from the load wire for MA experiments.

For outflows with a target, shocks form largely in the same way for each system. The plasma flow is highly collisional and supersonic ($M > 2.5$) and generates a clear Mach cone. The Drake shock parameter Q ($>10^4$) and radiative parameter R_r ($>10^2$) are high in all cases. A significant difference is the effect radiation plays on the energy balance in the flow upstream of the shock region. At sufficiently high densities (COBRA), radiation causes pre-heat of the flow several millimeters ahead of the shock region as measured with Thomson

scattering. At lower densities, radiation is simply lost as the photon mean free path is very long compared to the shock scale length ($\sim$100 μm), and upstream heating of the plasma is not observed. These observations compare well to previous data at intermediate densities on the XP generator at Cornell and to analytical calculations.

ACKNOWLEDGMENT

The authors thank Todd Blanchard and Harry Wilhelm for engineering support for the COBRA experiments performed at Cornell University. They also thank the referees for their thorough review of their manuscript and several useful suggestions.

REFERENCES

[1] J. von Neumann, Dept. Navy, Bur. Ordnance, Washington, DC, USA, Explos. Res. Rep. 12, 1943, pp. 238–299.
[2] G. Ben-Dor, *Shock Wave Reflection Phenomena*. Berlin, Germany: Springer, 2007.
[3] P. Hartigan et al., "When shock waves collide," *Astrophys. J.*, vol. 823, no. 2, p. 148, Jun. 2016.
[4] K. Yirak et al., "Mach stem hysteresis: Experiments addressing a novel explanation of clumpy astrophysical jet emission," *High Energy Density Phys.*, vol. 9, no. 2, pp. 251–257, Jun. 2013.
[5] G. W. Collins et al., "Measurements of the equation of state of deuterium at the fluid insulator-metal transition," *Science*, vol. 281, no. 5380, pp. 1178–1181, Aug. 1998.
[6] J. A. Gaffney et al., "A review of equation-of-state models for inertial confinement fusion materials," *High Energy Density Phys.*, vol. 28, pp. 7–24, Sep. 2018.
[7] D. H. Munro et al., "Shock timing technique for the national ignition facility," *Phys. Plasmas*, vol. 8, no. 5, pp. 2245–2250, May 2001.
[8] R. Betti, C. D. Zhou, K. S. Anderson, L. J. Perkins, W. Theobald, and A. A. Solodov, "Shock ignition of thermonuclear fuel with high areal density," *Phys. Rev. Lett.*, vol. 98, no. 15, Apr. 2007, Art. no. 155001.
[9] P. Wang et al., "Density-dependent shock Hugoniot of polycrystalline diamond at pressures relevant to ICF," *Matter Radiat. Extremes*, vol. 6, no. 3, May 2021, Art. no. 035902.
[10] P. Hartigan et al., "Fluid dynamics of stellar jets in real time: Third epochhubble space telescopeimages of HH 1, HH 34, and HH 47," *Astrophys. J.*, vol. 736, no. 1, p. 29, Jul. 2011.
[11] B. Reipurth and J. Bally, "Herbig-haro flows: Probes of early stellar evolution," *Annu. Rev. Astron. Astrophys.*, vol. 39, no. 1, pp. 403–455, Sep. 2001.
[12] E. A. Helder, D. Kosenko, and J. Vink, "Cosmic-ray acceleration efficiency versus temperature equilibration: The case of SNR 0509-67.5," *Ap. J. Lett.*, vol. 719, no. 2, pp. L140–L144, 2010.
[13] P. Ghavamian, J. M. Laming, and C. E. Rakowski, "A physical relationship between electron-proton temperature equilibration and Mach number in fast collisionless shocks," *Astrophys. J.*, vol. 654, no. 1, p. L69, 2007.
[14] M. D. Knudson et al., "Probing the interiors of the ice giants: Shock compression of water to 700 GPa and 3.8 g/cm^3," *Phys. Rev. Lett.*, vol. 108, no. 9, Feb. 2012, Art. no. 091102.
[15] A. J. Harvey-Thompson et al., "Quantitative analysis of plasma ablation using inverse wire array Z pinches," *Phys. Plasmas*, vol. 16, no. 2, Feb. 2009, Art. no. 022701.
[16] J. T. Banasek, T. G. Oliver, S. W. Cordaro, and S. C. Bott-Suzuki, "Free space Thomson scattering to study high energy density shocks," *Rev. Sci. Instrum.*, vol. 92, no. 9, Sep. 2021, Art. no. 093503.
[17] J. B. Greenly, J. D. Douglas, D. A. Hammer, B. R. Kusse, S. C. Glidden, and H. D. Sanders, "A 1MA, variable risetime pulse generator for high energy density plasma research," *Rev. Sci. Instrum.*, vol. 79, no. 7, Jul. 2008, Art. no. 073501.
[18] S. V. Lebedev et al., "Effect of discrete wires on the implosion dynamics of wire array z pinches," *Phys. Plasmas*, vol. 8, no. 8, pp. 3734–3747, Aug. 2001.
[19] S. C. Bott et al., "Experimental analysis of the acceleration region in tungsten wire arrays," *IEEE Trans. Plasma Sci.*, vol. 40, no. 12, pp. 3324–3328, Dec. 2012.
[20] M. E. Cuneo et al., "Characteristics and scaling of tungsten-wire-array z-pinch implosion dynamics at 20 MA," *Phys. Rev.*, vol. 71, no. 4, 2005, Art. no. 046406.
[21] R. D. McBride et al., "Implosion dynamics and radiation characteristics of wire-array Z pinches on the cornell beam research accelerator," *Phys. Plasmas*, vol. 16, no. 1, Jan. 2009, Art. no. 012706.
[22] S. C. Bott-Suzuki et al., "Investigation of radiative bow-shocks in magnetically accelerated plasma flows," *Phys. Plasmas*, vol. 22, no. 5, May 2015, Art. no. 052710.
[23] *ThomsonPy Code Repository*. Accessed: Nov. 2018. [Online]. Available: https://github.com/jbano2/thomsonpy
[24] J. T. Banasek, T. Byvank, S. V. R. Rocco, W. M. Potter, B. R. Kusse, and D. A. Hammer, "Time-resolved Thomson scattering on laboratory plasma jets," *IEEE Trans. Plasma Sci.*, vol. 46, no. 11, pp. 3901–3905, Nov. 2018.
[25] J. T. Banasek et al., "Current polarity effects on laboratory plasma jets," *Phys. Plasmas*, vol. 28, no. 8, Aug. 2021, Art. no. 082703.
[26] J. T. Banasek et al., "Probing local electron temperature and density inside a sheared flow stabilized Z-pinch using portable optical Thomson scattering," *Rev. Sci. Instrum.*, vol. 94, no. 2, Feb. 2023, Art. no. 023508, doi: 10.1063/5.0135265.
[27] M. P. Valdivia et al., "Current advances on Talbot–Lau X-ray imaging diagnostics for high energy density experiments (invited)," *Rev. Sci. Instrum.*, vol. 93, no. 11, Nov. 2022, Art. no. 115102.
[28] G. Pérez-Callejo et al., "TIA: A forward model and analyzer for Talbot interferometry experiments of dense plasmas," *Phys. Plasmas*, vol. 29, no. 4, Apr. 2022, Art. no. 043901.
[29] M. P. Valdivia et al., "Z-pinch interferometry analysis with the Fourier-based TNT code," *IEEE Trans. Plasma Sci.*, early access, Aug. 12, 2024, doi: 10.1109/TPS.2024.3420910.
[30] J. P. Chittenden, S. V. Lebedev, B. V. Oliver, E. P. Yu, and M. E. Cuneo, "Equilibrium flow structures and scaling of implosion trajectories in wire array z pinches," *Phys. Plasmas*, vol. 11, no. 3, pp. 1118–1127, Mar. 2004.
[31] S. C. Bott et al., "Study of the effect of current rise time on the formation of the precursor column in cylindrical wire array Z pinches at 1 MA," *Phys. Plasmas*, vol. 16, no. 7, Jul. 2009, Art. no. 072701.
[32] S. C. Bott et al., "Dynamics of cylindrically converging precursor plasma flow in wire-array z-pinch experiments," *Phys. Rev. E, Stat. Phys. Plasmas Fluids Relat. Interdiscip. Top.*, vol. 74, no. 4, Oct. 2006, Art. no. 046403.
[33] A. B. Reighard et al., "Observation of collapsing radiative shocks in laboratory experiments," *Phys. Plasmas*, vol. 13, no. 8, Aug. 2006, Art. no. 082901.
[34] R. P. Drake, "Theory of radiative shocks in optically thick media," *Phys. Plasmas*, vol. 14, no. 4, Apr. 2007, Art. no. 043301.
[35] R. P. Drake, "Energy balance and structural regimes of radiative shocks in optically thick media," *IEEE Trans. Plasma Sci.*, vol. 35, no. 2, pp. 171–180, Apr. 2007.
[36] G. D. Tsakiris and K. Eidmann, "An approximate method for calculating Planck and Rosseland mean opacities in hot, dense plasmas," *J. Quant. Spectrosc. Radiat. Transf.*, vol. 38, no. 5, pp. 353–368, Nov. 1987.

Simon C. Bott-Suzuki (Senior Member, IEEE) received the M.Phys. degree in chemical physics and the Ph.D. degree in physics from Sheffield University, Sheffield, U.K., in 1999 and 2004, respectively.

He subsequently carried out post-doctoral research at Imperial College London, London, U.K., before moving to the University of California San Diego, La Jolla, CA, USA, in 2006. He is currently an Associate Research Scientist with the Center for Energy Research, UC San Diego; a Visiting Professor with Cornell University, Ithaca, NY, USA; and a Visiting Scientist with Lawrence Livermore National Laboratories, Livermore, CA, USA. He presently leads the Pulsed Plasma Physics (P3) Group, which investigates plasmas generated using pulsed power techniques and their application in inertial fusion energy, basic plasma physics, and laboratory astrophysics. He has authored over 70 journal articles, in high-energy-density science, novel experimental platforms, pulsed dower driver development, and plasma diagnostics.

Dr. Bott-Suzuki served as the Co-Chair for the 9th International Conference on Dense Z-Pinches (Napa, CA 2014). He has also served in various roles for the ICOPS conference series and as the Guest Editor for the Fourth and Fifth Special Issues on Z-pinch plasmas published in IEEE TRANSACTIONS ON PLASMA SCIENCE.

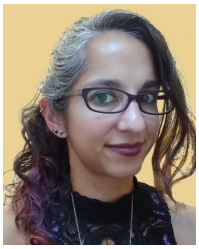

Maria Pia Valdivia (Member, IEEE) received the Ph.D. degree in exact sciences from the Pontificia Universidad Católica de Chile, Santiago, Chile, in 2011.

She is an Assistant Research Scientist at the Center for Energy Research, University of California at San Diego, La Jolla, CA, USA, and a Visiting Research Scientist at the Department of Physics and Astronomy, Johns Hopkins University, Baltimore, MD, USA. Her research interests include high-energy-density laboratory plasmas in high-intensity laser and pulsed power systems and the development of advanced high-temperature plasma diagnostics. She is also involved in informal education programs; physics education research; and diversity, equity, inclusion, and accessibility initiatives.

Jacob T. Banasek (Member, IEEE), photograph and biography not available at the time of publication.

Samuel W. Cordaro (Member, IEEE), photograph and biography not available at the time of publication.

Ann Truong, photograph and biography not available at the time of publication.

Hanyu Hu, photograph and biography not available at the time of publication.

Chin-Chou Wu, photograph and biography not available at the time of publication.

Noah Dilworth, photograph and biography not available at the time of publication.

B. R. Kusse, photograph and biography not available at the time of publication.

D. A. Hammer (Life Fellow, IEEE), photograph and biography not available at the time of publication.

Eric Sander Lavine (Member, IEEE) received the Ph.D. degree from the Aeronautics and Astronautics Department, University of Washington, Seattle, WA, USA, in 2018, for his work on the MOCHI.LabJet experiment, an astrophysical-relevant laboratory plasma jet with self-organized magnetic fields and stabilizing helical shear flows.

He joined the Cornell Laboratory of Plasma Studies, Ithaca, NY, USA, in spring of 2018, as a Post-Doctoral Research Associate, focusing on the dynamics and stability of gas-puff Z-pinch implosions. Currently, as an Assistant Research Professor, his additional research interests include laboratory astrophysics (jets, shocks, and turbulence), plasma relaxation and self-organization, power flow, and diagnostic development.

W. M. Potter (Member, IEEE), photograph and biography not available at the time of publication.

J. B. Greenly (Member, IEEE), photograph and biography not available at the time of publication.

Felipe Veloso (Member, IEEE) received the B.Sc. and Ph.D. degrees in physics from the Pontificia Universidad Católica de Chile, Santiago, Chile, in 2002 and 2008, respectively.

In 2012, he joined Pontificia Universidad Católica de Chile, as Faculty Member, where he is currently an Associate Professor. His research interests include experimental plasma physics using Z-pinches, laboratory astrophysics, and plasma diagnostics techniques, among others. He is also interested in physics and science education to diverse audiences.